Directional emission from dye-functionalized plasmonic DNA superlattice microcavities

Daniel J. Park[a,b,1], Jessie C. Ku[b,c,1], Lin Sun[b,c], Clotilde M. Lethiec[a], Nathaniel P. Stern[d], George C. Schatz[a,b,2], and Chad A. Mirkin[a,b,c,2]

[a]Department of Chemistry, Northwestern University, Evanston, IL 60208; [b]International Institute for Nanotechnology, Northwestern University, Evanston, IL 60208; [c]Department of Materials Science and Engineering, Northwestern University, Evanston, IL 60208; and [d]Department of Physics and Astronomy, Northwestern University, Evanston, IL 60208

Three-dimensional plasmonic superlattice microcavities, made from programmable atom equivalents comprising gold nanoparticles functionalized with DNA, are used as a testbed to study directional light emission. DNA-guided nanoparticle colloidal crystallization allows for the formation of micrometer-scale single-crystal body-centered cubic gold nanoparticle superlattices, with dye molecules coupled to the DNA strands that link the particles together, in the form of a rhombic dodecahedron. Encapsulation in silica allows one to create robust architectures with the plasmonically active particles and dye molecules fixed in space. At the micrometer scale, the anisotropic rhombic dodecahedron crystal habit couples with photonic modes to give directional light emission. At the nanoscale, the interaction between the dye dipoles and surface plasmons can be finely tuned by coupling the dye molecules to specific sites of the DNA particle-linker strands, thereby modulating dye–nanoparticle distance (three different positions are studied). The ability to control dye position with subnanometer precision allows one to systematically tune plasmon–exciton interaction strength and decay lifetime, the results of which have been supported by electrodynamics calculations that span length scales from nanometers to micrometers. The unique ability to control surface plasmon/exciton interactions within such superlattice microcavities will catalyze studies involving quantum optics, plasmon laser physics, strong coupling, and nonlinear phenomena.

DNA programmable assembly | directional emission | anisotropic 3D microcavity | nanoparticle surface plasmon | fluorescence enhancement

Microcavities are important photonic architectures that can be used to couple dipole emitters with optical modes and enhance light–matter interactions typically with long cavity lifetimes (high Q factors). They have been used to understand phenomena in cavity quantum electrodynamics (1, 2), and to enable molecular sensing (3) and lasing (4) technologies. In recent years, researchers have developed strategies for incorporating plasmonic nanostructures into microcavity structures to enhance light–matter interactions via strong light confinement (small mode volume, V), resulting in materials that are capable of plasmon lasing (5–7). These plasmonic microcavities exploit two different aspects of the architectures simultaneously: guided optical modes that resonate or scatter light (via the microcavity geometry) and near-field–driven optical confinement (via the metallic nanostructure). Such hybrid photonic structures are desirable because they can lead to high Q factors and strong light confinement within a single architecture, significantly enhancing light–matter interactions by a large cavity figure of merit, Q/V. However, most of the plasmonic microcavities have been limited to 1D or 2D microcavity geometries and plasmonic mode confinement (7) (metallic nanostructures) due to limitations in fabrication methods (6, 8). Importantly, 3D counterparts of these 1D and 2D architectures can lead to interesting properties such as higher microcavity Q factors (2), 3D angular emission dependence, and stronger mode confinement (7).

DNA-guided nanoparticle colloidal crystallization provides remarkable control over the assembly of nanoparticles into superlattices (9, 10), enabling the deliberate tailoring of crystal symmetry (9), lattice constant (11), and particle composition (12). Furthermore, structures with geometrically well-defined 3D crystal habits (10), when locked into the solid state via silica embedding procedures (13), open up potential applications in the field of optics. Therefore, these methods provide exciting possibilities for controlling the interaction between photonic modes of microcavity structures and plasmonic modes of the highly polarizable nanoparticles for nano-/micrometer-scale optical applications. Indeed, it was recently demonstrated that one can control the strength of coupling between Fabry–Perot modes and localized surface plasmons in a body-centered cubic (bcc) crystal composed of gold nanoparticles with a rhombic dodecahedron (RD) crystal habit (14). Such superstructures behave as 3D plasmonic microcavities (passive cavities) that exhibit both guided modes and plasmonic near-field effects throughout the cavity medium. Therefore, upon incorporating excitonic materials into these superlattices, the nature of such 3D plasmonic microcavities (active cavities) can be explored systematically through an analysis of excitonic emission properties.

In this work, we synthesize dye-functionalized plasmonic superlattices via DNA programmable assembly (10, 14), and study their emission properties both experimentally and theoretically.

Significance

In this article, we use microscopic rhombic dodecahedra made from DNA-programmable assembly of programmable atom equivalents (i.e., DNA-functionalized nanoparticles), to study the importance of nano- and microscopic architecture on directional light emission. The DNA sequence design provides subnanometer control over the interactions between light-emitting molecules and metal nanoparticles, resulting in micrometer-scale light–matter interactions which induce unique spatial and spectral emission profiles. Electrodynamics calculations combining the two scales successfully model the observed behaviors. This initial study provides a compelling demonstration of the utility of DNA-programmable assembly for making 3D photonic devices that uniquely allow one to engage in structure–function relationship studies, important in fields spanning quantum electrodynamics and plasmonics.

CHEMISTRY

Fig. 1. Scheme showing the 3D microcavity geometry (blue, *Bottom Right*) and a dye-coupled gold nanoparticle (magenta, *Top*) of dye-functionalized single-crystal bcc superlattices. An SEM image shows a representative superlattice (*Bottom Left*). The superlattice is drop-cast onto a glass substrate leading to a facet facing up orientation (*Bottom Right*). Its RD shape can lead to 3D microcavity properties. $\vec{L}$ is defined as a vector connecting two vertices (two red dots) with the largest intervertex distance (blue arrow aligned with *y* axis, *Bottom Right*). Three $\vec{L}$s can be defined in an RD, and they all pass through the center of the structure. The gold nanoparticles at the lattice sites in the superlattice (*Top*) are surrounded by multiple dye molecules forming a layer, and the distance between the gold surface and the dye layer is controlled by selecting a dye binding site among three sites (purple circles; denoted d1, d2, and d3 from left to right) on DNA strands (*Dye-Coupled Plasmonic Superlattice Microcavity Fabrication*, *Dye-Labeled DNA Synthesis*, and *Dye-Coupled Plasmonic Superlattice Microcavity Fabrication*, *DNA Nanoparticle Conjugate Preparation*). The dye molecules are chosen based on the spectral positions of their emission with respect to that of the surface plasmons, depending on the intended use.

The plasmonic microcavity emission behavior of these crystals is first investigated via a spatio-spectral analysis, and the ability to control the interaction between plasmonic nanoparticles and dye

excitons via dye placement within the structure is studied by decay lifetime measurements.

To construct a dye-functionalized plasmonic microcavity, bcc superlattices with a 52-nm lattice constant were synthesized from DNA-functionalized 20-nm-diameter gold nanoparticles (Fig. 1; see *Dye-Coupled Plasmonic Superlattice Microcavity Fabrication*, *Dye-Labeled DNA Synthesis* and *Dye-Coupled Plasmonic Superlattice Microcavity Fabrication*, *DNA Nanoparticle Conjugate Preparation*). Such structures have a gold volume fraction (*FF*) of about 6%. A scanning electron microscope (SEM) image confirms the micrometer size of the crystals and the well-defined RD crystal habit (Fig. 1, *Bottom*). To describe the crystal orientations in this work, $\vec{L}$ is defined as the vector connecting two vertices with the largest intervertex distance (Fig. 1, *Bottom Right*). The RD crystal habit can induce anisotropic microcavity properties (15) due to its geometry. Specifically, light emitted from the dye–Au nanoparticle complexes (lattice sites) can be scattered by the RD architecture leading to an angular dependence of the cavity emission profile in 3D. Simultaneously, due to internal reflection at facets of the RD habit, optical resonant modes can be established based on its intrinsic symmetry as in the case of its spherical counterpart (2, 3). Overall, these microcavity properties can be influenced by the plasmonic resonance of the nanoparticle lattice that modulates real and imaginary parts of the microcavity refractive index (14). To incorporate dye excitons at the nanoscale, DNA strands were synthesized with amino-modified dT bases where dye-labeled NHS esters can bind (Fig. 1, *Top* and Table S1). Specifically, to control the interaction between the dye excitons and plasmonic nanoparticles (16, 17), three dye-to-gold surface distances (1, 5, and 11 nm; denoted d1, d2, and d3, respectively) were used. In addition, Alexa Fluor 532 and 700 dyes were used to study the importance of spectral overlap between the dye (exciton) emission and the frequency of the localized surface plasmon resonance (LSPR; ~520 nm). Approximately 120 dye molecules were attached to each gold nanoparticle, as determined by fluorophore assays (*Supporting Information*). Due to the small

Fig. 2. Spatio-spectral analysis of microcavity dye emission. (*A*) Optical experiment setup for spatio-spectral analysis. Laser pulses (λ = 504 nm, pulse width ~100 ps, spot size of ~5–10 μm) were used in transmission mode and focused through a 100× objective lens to excite a single superlattice. The superlattice emission was collected with a 50× objective lens and spatio-spectral analysis was collected via a spectrometer and a CCD. Two filter sets, band-pass and long-pass, were used to narrow the pulsed laser linewidth and to reject part of the laser light. The focal plane of the 50× objective lens was tuned to generate data at multiple focal planes (dashed lines). The orientation of the superlattice and substrate are reversed from that depicted in Fig. 1 (*Bottom Right*), as their *z* axes indicate. Optical images show a bright-field image of a superlattice on a glass substrate with $\vec{L}$ denoted (blue arrow, *Top*) and the same superlattice illuminated by the pulse laser (*Bottom*). The white arrow indicates the slit location. (*B*) Spatio-spectral emission profile (*Left*) of a d1 superlattice ($L \sim 5$ μm, *Inset*) compared with the theoretical prediction (*Right*). The top images were formed with the focal plane located around the center of the superlattice and the bottom with the focal plane 3 μm below it (see the scheme in *A*). Emitted light was collected with a slit cutting through the center of the superlattice (white arrow in *A*) where spatial (vertical axis of the profile, 30 μm) and spectral information were collected (horizontal axis of the profile). (*C*) Comparable data for a gold-etched control d1 superlattice were investigated to analyze the effect of plasmonic absorbers. The gold-etched control superlattice is transparent due to lack of nanoparticle absorption (*Inset*). (Scale bar, 5 μm.)

size of the nanoparticles, lattice sites can be considered dipole emitters. The loading of fluorophores on our nanoparticles could give lower dye quantum yields and altered dye lifetimes due to energy transfer (17), but the low particle density is such that this should not influence the emission angular profile (and our modeling confirms this).

The plasmonic microcavity behavior of the silica encapsulated superlattices was probed with a pulsed laser coupled microspectrophotometry system (Fig. 2A and Fig. S1). A d1 superlattice with Alexa Fluor 532 dyes was chosen to determine the effect of superlattice microstructure on directional emission. Spatio-spectral emission data were collected from 515 to 800 nm to include the LSPR frequency to understand the surface plasmon contributions to emission behavior. A 50-μm slit was used to collect light from a thin line cutting through the superlattice center (Fig. 2A, white arrow) and also to provide spectral resolution. In the collection process, the long axes of the superlattices (Fig. 2A, blue arrow; $\vec{L}$ in Fig. 1, *Right*) were aligned with the slit to analyze the emitted light from an angle parallel to $\vec{L}$. The spatio-spectral emission profile of the superlattice with $L \sim 5$ μm (Fig. 2B, *Left*) shows a transition from a double-line shape to a triangular shape as the focal plane of the objective lens is moved away from the center of the superlattice (red arrows in Fig. 2 A and B). Such profiles (Fig. 2B, *Left*) are observed from single-crystal superlattices with well-formed RD crystal habits, whereas polycrystalline superlattices of random micrometer-scale shapes do not show such profiles (Fig. S2). To understand the effect of plasmonic nanoparticles in the microcavity, the same analysis was performed with a gold-etched control (and therefore gold-free) d1 superlattice (dielectric RD structure; Fig. 2C, *Inset*). Its spatio-spectral profile (Fig. 2C) does not exhibit the profile exhibited by its plasmonic counterpart (Fig. 2B, *Left*), and its emission spectral range is narrow ($\lambda \sim 550$–650 nm), similar to that of Alexa Fluor 532 free dye dissolved in water (*Theoretical Analysis of Superlattice Microcavity Emission Behavior*, *Quantum Yield* $[q(\lambda)]$ *and Enhanced Decay Rates of a Dye Around a Gold Nanoparticle; Fitting of the Theoretical Spatio-Spectral Emission Profile* $[T(\lambda, \vec{r})]$). These experiments demonstrate the strong near-field contributions of the plasmonic nanoparticles to the emission profile of the superlattice. Specifically, strong mode confinement and absorption (Fig. 2B) broaden and modify the spectral profile of exciton emission (7).

To understand this superlattice emission behavior (Fig. 2B), finite-difference time-domain (FDTD) (18) simulations and nanophotonic calculations (17, 19) were performed to explain the effects of RD microcavity scattering and nanoparticle surface plasmons, respectively (*Theoretical Analysis of Superlattice Microcavity Emission Behavior* and Fig. S3). The FDTD electrodynamics simulations were performed using dipole sources in an RD geometry to simulate emission from individual lattice sites (Fig. 3; *Theoretical Analysis of Superlattice Microcavity Emission Behavior*, *Microcavity Scattering Profile* $[G_{RD}(\lambda, \vec{r})]$; *Theoretical Analysis of Superlattice Microcavity Emission Behavior*, *Excitation Laser Intensity Profile in Microcavity* $[I(\lambda_{exc}, \vec{r}_{exc})]$; and *Theoretical Analysis of Superlattice Microcavity Emission Behavior*, *EMT Approximation*). Because each lattice site is a gold nanoparticle surrounded by a dye layer, each site can be considered a plasmonically influenced dipole emitter (16, 17). Importantly, the superlattices were illuminated in transmission mode in the experiment (Fig. 2A). The laser can only excite a limited volume of the superlattice on the illuminated side (bottom of superlattice in Fig. 3 and Fig. S4; *Theoretical Analysis of Superlattice Microcavity Emission Behavior*, *Excitation Laser Intensity Profile in Microcavity* $[I(\lambda_{exc}, \vec{r}_{exc})]$; and *Theoretical Analysis of Superlattice Microcavity Emission Behavior*, *EMT Approximation*) because the laser light ($\lambda \sim 504$ nm) strongly couples to surface plasmons of the nanoparticles and is absorbed. Therefore, the observed profiles (Fig. 2B) are constructed by emission from the
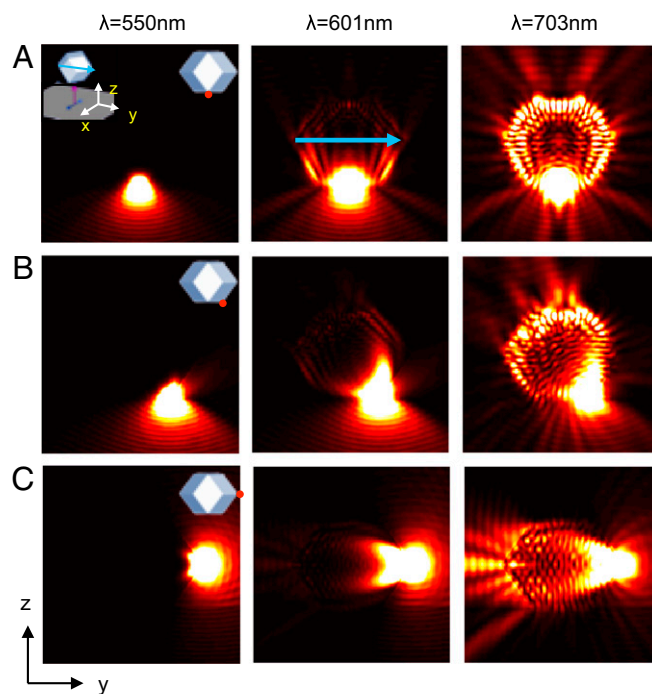

Fig. 3. Simulated microcavity near-field emission profiles. (A) FDTD-simulated near-field emission profile ($|\vec{E}|^2$) of a dipole at the bottom of a superlattice microcavity. The microcavity center is $(x,y,z) = (0,0,0)$, L is 5 μm, and the gold FF is 6%. (*Left Inset*) Microcavity orientation with respect to the coordinates as in Fig. 1. The incident direction of the excitation laser is indicated by a red arrow below the RD geometry. (*Right Inset*) Dipole (red dot) location, in the y–z plane, at the bottom of the RD geometry right beneath the facet. $\vec{L}$ is indicated by a blue arrow. Three dipole orientations aligned with the x, y, and z axes were used and $|\vec{E}|^2$ were averaged incoherently over these orientations. Three wavelengths are presented to show the behaviors close to and away from the LSPR frequency. Intensity around each dipole was purposely saturated based on the same scaling scheme to show light scattering throughout the RD shape. A substrate ($n = 1.44$) was added below the RD shape. (B and C) The same type of data as in A for two other dipole locations. All of the dipole sources were in the y–z plane beneath the surface of the RD shapes. See Fig. S6 for emission profiles in the x–z plane.

excited volumes. Near-field profiles of single-dipole emission in the excited volume reveal strong spectral dependence of light transmission through the superlattice (Fig. 3 and Figs. S5 and S6). Near the LSPR frequency, emitted light is mostly directed away from the superlattice and only shallow penetration into the superlattice is observed due to strong plasmonic absorption (Fig. 3, *Left*). Far from the LSPR frequency (>600 nm, Fig. 3, *Right*), the light is transmitted through the superlattice and then emitted in various directions that are determined by the photonic properties of the RD, similar to what might be expected for a dielectric microcavity. Interestingly, depending on the position of the dipoles, high near-field intensity is observed just beneath the surface of the RD (Fig. 3A, *Right* and Fig. S6). This is due to internal reflection and indicates the existence of resonant modes similar to whispering-gallery modes (WGMs) found in spherical microcavities (2, 3). Such modes with the RD shape should not be surprising because WGMs exist in various 2D anisotropic microcavities (15, 20), and not just in circular ones. These observations suggest the possibility of using such architectural control to design 3D plasmonic microcavities with spatially and spectrally defined emission properties. Indeed, the RD shape can result in complex 3D WGMs at wavelengths longer than the LSPR frequency, and when such lattices are combined with a silver coating, moderate Q factors ($>10^2$) are possible (14). Importantly, the controllable exciton–plasmon interaction afforded

by DNA-directed assembly makes it possible to exploit two intrinsically different cavity functions: the strong plasmonic near field around the LSPR wavelength (the dye–particle interaction), and the dielectric-cavity behavior at wavelengths longer than the LSPR frequency (the RD crystal habit).

Based on the predicted microcavity scattering behavior in the near field (Fig. 3), theoretical spatio-spectral profiles (Fig. 2B, *Right*) were constructed to explain the directional emission of the superlattice microcavities. In this process, the near-field scattering profiles of multiple dipoles at the bottom of the microcavity were projected into the far field (*Theoretical Analysis of Superlattice Microcavity Emission Behavior*, *Microcavity Scattering Profile [$G_{RD}(\lambda, \vec{r})$]*; and *Theoretical Analysis of Superlattice Microcavity Emission Behavior*, *Excitation Laser Intensity Profile in Microcavity [$I(\lambda_{exc}, \vec{r}_{exc})$]*). The intrinsic dye emission spectrum (Alexa Fluor 532) and the nanoscale effect of coupling the dye to surface plasmons (leading to both enhancement and suppression of fluorescence) were incorporated into our theoretical models (*Theoretical Analysis of Superlattice Microcavity Emission Behavior*, *Quantum Yield [$q(\lambda)$] and Enhanced Decay Rates of a Dye Around a Gold Nanoparticle; Fitting of the Theoretical Spatio-Spectral Emission Profile [$T(\lambda, \vec{r})$]*) (17, 19). Significantly, at long wavelengths and with the superlattice out of focus, the superlattice profile (Fig. 2B, *Bottom*) shows high intensity at the center of the superlattice. Careful FDTD analysis at multiple focal plane positions (Fig. S7) reveals a clear light convergence in front of the microcavity. This is due to the directional scattering behavior of the microcavity which vertically projects and focuses emitted light from the excited volume (Fig. 3 A and B, *Right* and Fig. S6). On the other hand, emitted light from the side vertices (Fig. 3C, *Right*), which couples to the microcavity, is projected horizontally, and therefore, is not detected by the objective lens at long wavelengths. Close to the LSPR wavelength, emitted light from the side vertices is clearly visible (Fig. 2B, *Bottom*) due to strong plasmon-driven light emission in three dimensions (Fig. 3C, *Left*). On the other hand, the intensity at the center of the microlens close to the LSPR wavelength is very low for all focal planes (Fig. 2B and Fig. S7) due to light absorption by surface plasmons (Fig. 3, *Left*). These spectrally modulated directional scattering behaviors are the result of the combined effects of the RD microcavity shape and the plasmonic nature of the microcavity medium. These properties of the microcavities are important and may prove useful for constructing light-emitting devices with plasmon-driven spectral modulation and directional light emission. Indeed, the 3D geometry-driven lensing effect can focus light close to the superlattice without additional micro-optical elements, thereby functioning as a local light source in larger devices. The spectral modulation provides tunability, allowing one to change the nature of light emission from scattered patterns (close to the LSPR frequency) to vertically/horizontally collimated ones (far from the LSPR frequency) by properly choosing the dye wavelength.

With these superlattice microcavities, one can systematically control the dye-to-gold nanoparticle distance by adjusting the point of covalent attachment of the dye to the DNA linker strands (Fig. 1, *Left*). Such control allows one to finely tune exciton–plasmon interactions (16, 17), which is important for emission engineering (7, 16) in regard to various parameters of interest such as decay rate and quantum efficiency. Microcavities with plasmonically active nanomaterials confined in 3D (nanoparticles) can exhibit orders-of-magnitude better light confinement (7) compared with 1D or 2D counterparts (e.g., nanosheets and nanorods). Therefore, nanophotonic calculations focused on exploring nanoparticle dye–exciton interactions (as described in *Theoretical Analysis of Superlattice Microcavity Emission Behavior*, *Quantum Yield [$q(\lambda)$] and Enhanced Decay Rates of a Dye Around a Gold Nanoparticle; Fitting of the Theoretical Spatio-Spectral Emission Profile [$T(\lambda, \vec{r})$]*, Fig. 4 A and B, and Figs. S8 and S9) show large decay enhancement factors at shorter wavelengths (<600 nm), with strong LSPR absorption (Fig. 4B). By carefully choosing the dye–gold surface distance via DNA design and the dye emission frequency, the quantum efficiency and the enhancement factor can both be optimized for desired applications.

To demonstrate the tunability of exciton–plasmon interactions, superlattices were also synthesized with Alexa Fluor 700 dye. Alexa Fluor 700 was chosen to avoid extremely high enhancement factors associated with metal absorption around the LSPR frequency (Fig. 4B), which would cause the dye lifetime to fall below the instrumental detection limit and result in low quantum efficiencies. Measurement of time-resolved emission using a time-correlated single-photon counting (TCSPC) system (*Optical Experiments*, *Single Superlattice Decay Lifetime Measurement* and Fig. S8) shows a dramatic reduction in lifetime from the control sample (dyes coupled to DNA strands in silica), to the d3 superlattice, and further to the d1 superlattice (Fig. 4C). Here, the d1 superlattice lifetime is at or below the
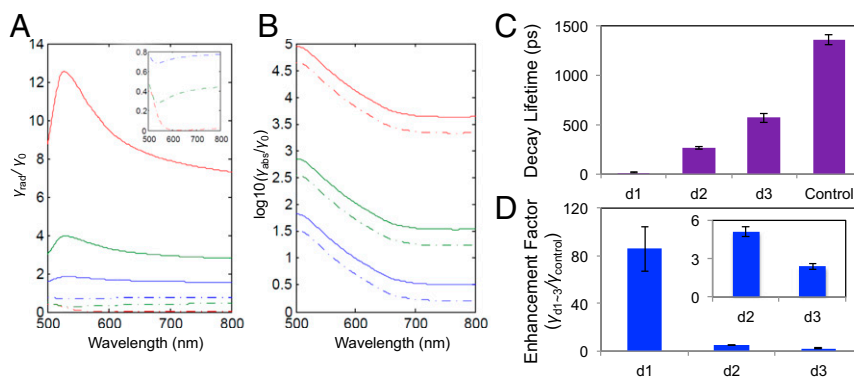

Fig. 4. Nanoparticle influenced dye temporal response. (A) Theoretically predicted (17) plasmon-enhanced radiative decay rates of dipoles normalized by their intrinsic radiative decay rate. Three different dye-to-nanoparticle surface distances are shown (1, 5, and 11 nm; d1, d2, and d3; red, green, and blue, and see *Theoretical Analysis of Superlattice Microcavity Emission Behavior*, *Quantum Yield [$q(\lambda)$] and Enhanced Decay Rates of a Dye Around a Gold Nanoparticle; Fitting of the Theoretical Spatio-Spectral Emission Profile [$T(\lambda, \vec{r})$]*). Solid lines (dashed lines) indicate perpendicular (parallel) dipole orientations. (B) A similar data set for absorption (nonradiative) decay rates as in A. (C and D) Measured decay lifetimes and corresponding enhancement factors of d1–d3 superlattices with Alexa Fluor 700 dye. Photons were collected at 700 nm by a TCSPC system coupled to the microspectrophotometer (*Optical Experiments*, *Single Superlattice Decay Lifetime Measurement* and Fig. 2A). Rapid rate enhancement was observed as the dye–nanoparticle distance decreased. Decay lifetime of the Alexa Fluor 700 dye in silica was used to measure the intrinsic decay lifetime.

instrument detection limit (∼10 ps; *Methods*). The measured enhancement factors (Fig. 4*D*) were comparable to calculated values (Fig. 4 *A* and *B*) (17) and were also in range of observations made for similar nanostructures (16). Because the dye orientations with respect to gold surfaces are unknown, the observed lifetimes are likely values averaged over multiple dye orientations and perhaps influenced by dye–dye interactions (17). Although microcavity modes of the superlattices can contribute to the accelerated decay behavior (2), we ignore such effects in this work due to their low Q factor (5, 7). Further investigation is necessary to correlate the effect of microcavity modes on Purcell factors (∼Q/V) by increasing Q factors with higher gold volume fractions or silver surface-coated systems (14). Such superlattice microcavities can function as 3D hybrid plasmonic microcavities that exhibit both WGMs with high Q factors and strong mode confinement of nanoparticles (small V) with a wide spectral range (7), leading to high Purcell factors (∼Q/V) for applications such as plasmon lasing.

This work has laid the foundation for preparing dye-functionalized DNA plasmonic nanoparticle superlattices with unusual optical properties that derive from the microscale crystalline architectures and the placement of the molecular and nanoscale components within such architectures. These initial proof-of-concept structures unambiguously show that one can obtain plasmonically modulated directional light emission. Moreover, the exciton–plasmon coupling can be fine-tuned by using the DNA linkers as programmable scaffolds to strategically position both the particles and the dyes. The DNA-guided approach to superlattice microcavities described herein provides a versatile platform for building photonic architectures with exciton emission behavior that can be modulated in the spatial, spectral, and time domains for various nano-/microphotonic applications.

Methods

FDTD Calculation. The FDTD simulations were performed with Lumerical FDTD solutions v.8.12.

Effective Medium Theory Approximation. Effective medium theory (EMT) approximation is used to approximate the refractive indices of superlattices based on the Maxwell–Garnett equation, $(\varepsilon_{eff} - \varepsilon_{host})/(\varepsilon_{eff} + 2\varepsilon_{host}) = FF[(\varepsilon_{inc} - \varepsilon_{host})/(\varepsilon_{inc} + 2\varepsilon_{host})]$, where ε_{eff}, ε_{inc}, and ε_{host} are dielectric constants of superlattices, gold, and silica host medium, and FF is the gold volume fraction.

Optical Experiments. Microspectrophotometry was performed using a 504-nm pulsed laser (Picoquant). The measurements were made using a 50× objective (N.A. 0.8, Zeiss) and a CCD (Princeton Instruments) coupled to a spectrometer (Princeton Instruments). The signal was normalized by spectra of the CCD quantum efficiency and filter sets. Decay lifetime measurements were performed by coupling the microspectrophotometry system to a TCSPC system (Picoquant) via an optical fiber.

TCSPC Lifetime Detection Limit. Through discussions with Picoquant, the limit was confirmed to be ∼10 ps based on the time scales of the detector, the pulse laser, and the TCSPC electronics.

See *Supporting Information* for details of experimental and theoretical methods used in this work.

1. Yamamoto Y, Tassone F, Cao H (2000) *Semiconductor Cavity Quantum Electrodynamics* (Springer, Berlin), p viii, 154 pp.
2. Vahala KJ (2003) Optical microcavities. *Nature* 424(6950):839–846.
3. Vollmer F, Arnold S (2008) Whispering-gallery-mode biosensing: Label-free detection down to single molecules. *Nat Methods* 5(7):591–596.
4. Sandoghdar V, et al. (1996) Very low threshold whispering-gallery-mode microsphere laser. *Phys Rev A* 54(3):R1777–R1780.
5. Tame MS, et al. (2013) Quantum plasmonics. *Nat Phys* 9(6):329–340.
6. Oulton RF, et al. (2009) Plasmon lasers at deep subwavelength scale. *Nature* 461(7264):629–632.
7. Genov DA, Oulton RF, Bartal G, Zhang X (2011) Anomalous spectral scaling of light emission rates in low-dimensional metallic nanostructures. *Phys Rev B* 83(24):245312.
8. de Leon NP, et al. (2012) Tailoring light-matter interaction with a nanoscale plasmon resonator. *Phys Rev Lett* 108(22):226803.
9. Macfarlane RJ, et al. (2011) Nanoparticle superlattice engineering with DNA. *Science* 334(6053):204–208.
10. Auyeung E, et al. (2014) DNA-mediated nanoparticle crystallization into Wulff polyhedra. *Nature* 505(7481):73–77.
11. Jones MR, et al. (2010) DNA-nanoparticle superlattices formed from anisotropic building blocks. *Nat Mater* 9(11):913–917.
12. Zhang C, et al. (2013) A general approach to DNA-programmable atom equivalents. *Nat Mater* 12(8):741–746.
13. Auyeung E, Macfarlane RJ, Choi CH, Cutler JI, Mirkin CA (2012) Transitioning DNA-engineered nanoparticle superlattices from solution to the solid state. *Adv Mater* 24(38):5181–5186.
14. Park DJ, et al. (2015) Plasmonic photonic crystals realized through DNA-programmable assembly. *Proc Natl Acad Sci USA* 112(4):977–981.
15. Wiersig J (2003) Hexagonal dielectric resonators and microcrystal lasers. *Phys Rev A* 67(2):023807.
16. Reineck P, et al. (2013) Distance and wavelength dependent quenching of molecular fluorescence by Au@SiO2 core-shell nanoparticles. *ACS Nano* 7(8):6636–6648.
17. Bharadwaj P, Novotny L (2007) Spectral dependence of single molecule fluorescence enhancement. *Opt Express* 15(21):14266–14274.
18. Taflove A, Hagness SC (2005) *Computational Electrodynamics: The Finite-Difference Time-Domain Method* (Artech House, Boston), 3rd Ed, p xxii, 1006 pp.
19. Gersten J, Nitzan A (1981) Spectroscopic properties of molecules interacting with small dielectric particles. *J Chem Phys* 75(3):1139–1152.
20. Chang ASP, et al. (2007) Visible three-dimensional metallic photonic crystal with non-localized propagating modes beyond waveguide cutoff. *Opt Express* 15(13):8428–8437.
21. Bergman DJ (1978) Dielectric-constant of a composite-material - problem in classical physics. *Phys Rep* 43(9):378–407.
22. Ruppin R (2000) Evaluation of extended Maxwell-Garnett theories. *Opt Commun* 182(4-6):273–279.
23. Ross MB, Blaber MG, Schatz GC (2014) Using nanoscale and mesoscale anisotropy to engineer the optical response of three-dimensional plasmonic metamaterials. *Nat Commun* 5:4090.
24. Johnson PB, Christy RW (1972) Optical constants of noble metals. *Phys Rev B* 6(12):4370–4379.

CHEMISTRY